OPEN ACCESS

University of BRISTOL

Bellesi, M., Haswell, J. D., de Vivo, L., Marshall, W., Roseboom, P. H., Tononi, G., & Cirelli, C. (2018). Myelin modifications after chronic sleep loss in adolescent mice. *Sleep*, *41*(5), [zsy034]. https://doi.org/10.1093/sleep/zsy034

Peer reviewed version

License (if available):
Other

Link to published version (if available):
10.1093/sleep/zsy034

Link to publication record in Explore Bristol Research

PDF-document

University of Bristol - Explore Bristol Research
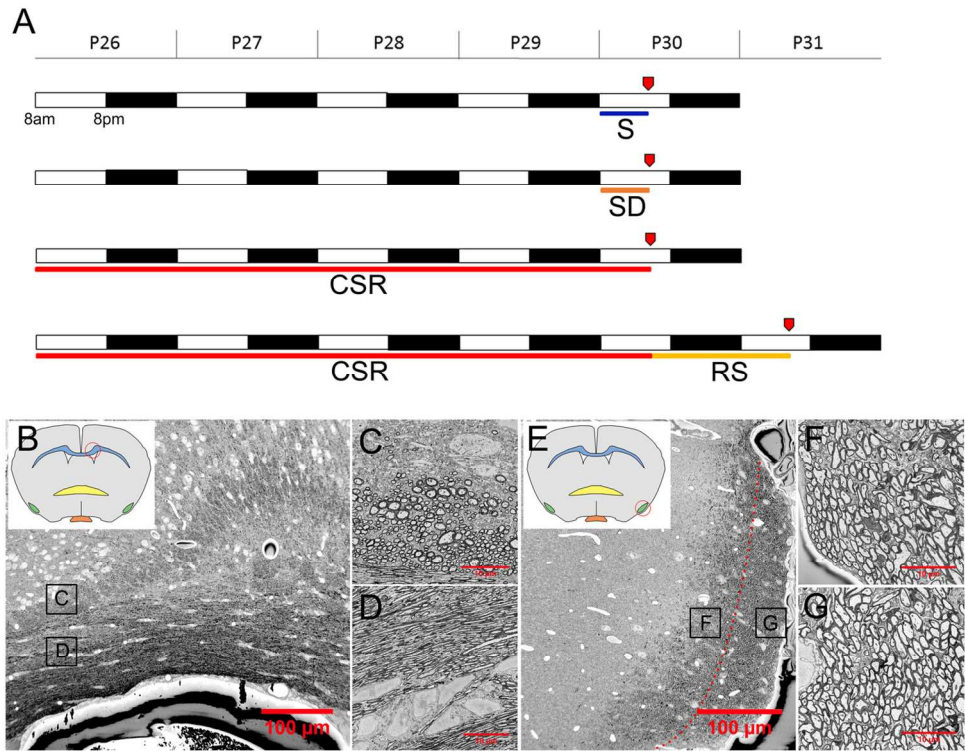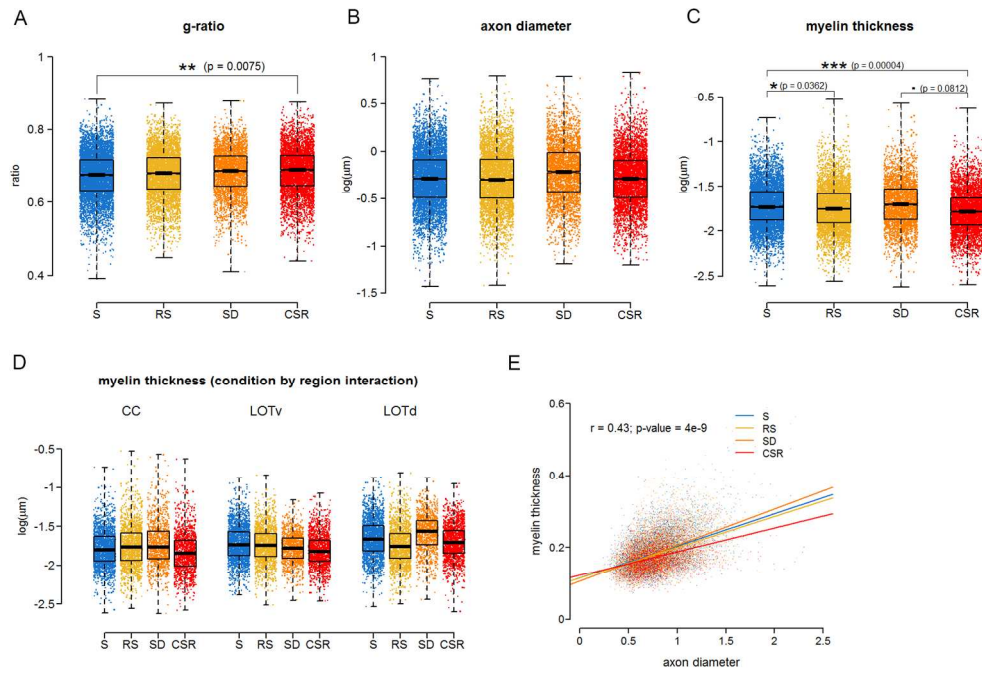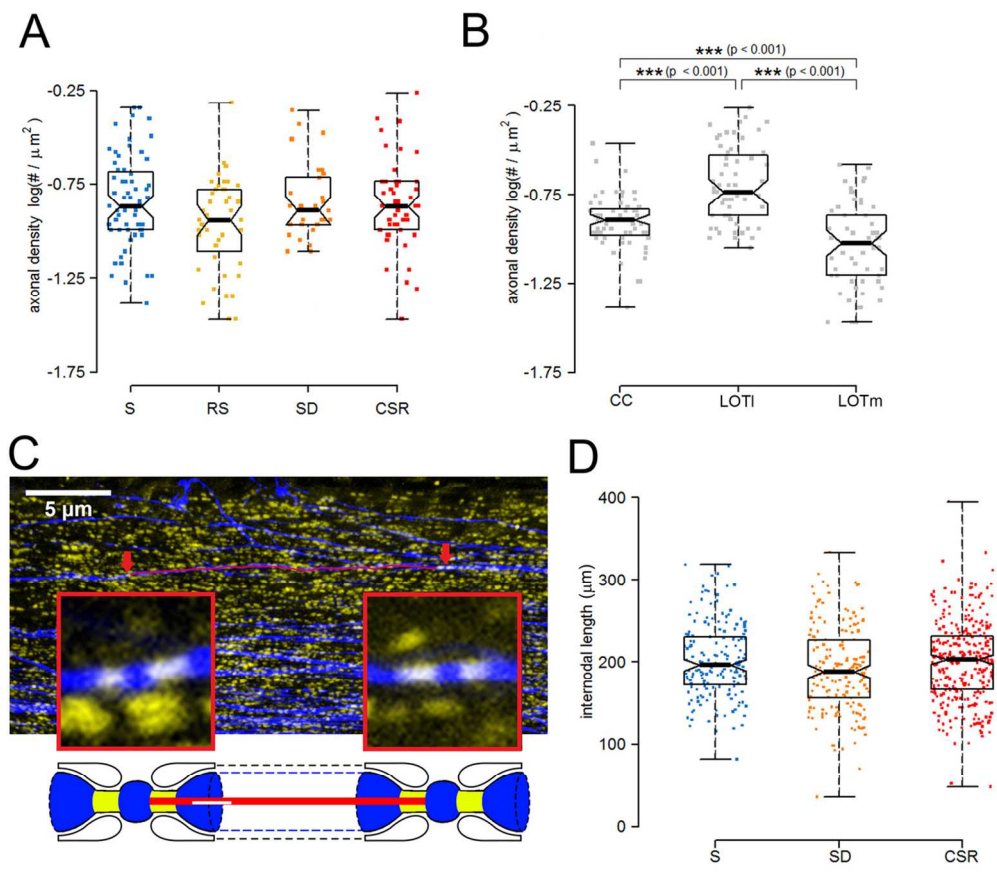**General rights**

Figure 1

130x98mm (300 x 300 DPI)

Revised Figure 2

632x419mm (72 x 72 DPI)

Bellesi-Haswell Figure 3 revised
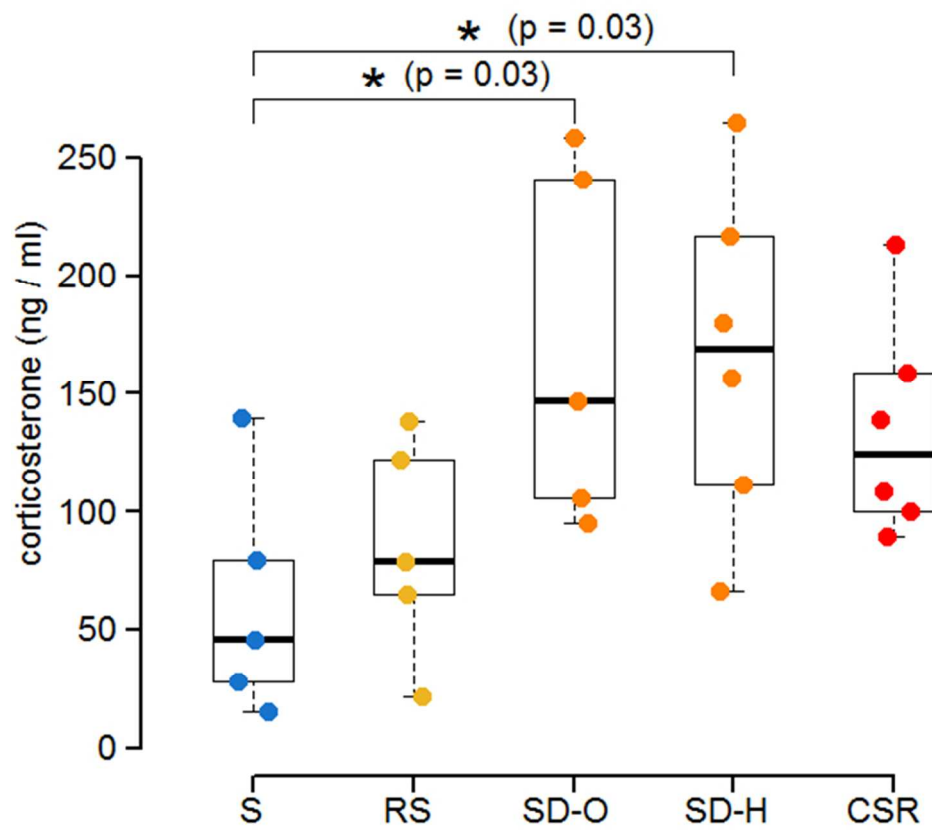
113x97mm (300 x 300 DPI)

Figure 4

211x186mm (72 x 72 DPI)

Myelin modifications after chronic sleep loss in adolescent mice

SUPPLEMENTARY MATERIALS

<u>Linear Mixed Effect Model – g-ratio.</u> The parameter estimates for the fixed effects model of *g-ratio*, including condition, region and their interaction are shown in Table S1.

Table S1: LME for g-ratio $^\wedge$ 2

Random Effects	Standard Error		
Mouse (Intercept)	0.0175		
Mouse (Region - LOTl)	0.0174		
Mouse (Region - LOTm)	0.0268		
Residual	0.0813		
Fixed Effects	**Level**	**Estimate**	**Standard Error**
Intercept		0.4532	0.0064
Condition	CSR (reference)	0	0
	SD	-0.0045	0.0069
	RS	-0.0102	0.0062
	S	-0.0185	0.0058
Region	CC (reference)	0	0
	LOTl	0.0193	0.0053
	LOTm	0.0424	0.0079

A power transformation (g-ratio $^\wedge$ 2) was applied to satisfy the model assumptions. Residual plots (shown below) were used to assess the model assumptions of normality and constant variance. From the scatter plot of residuals vs. fitted values, we found no evidence against either of the assumptions.
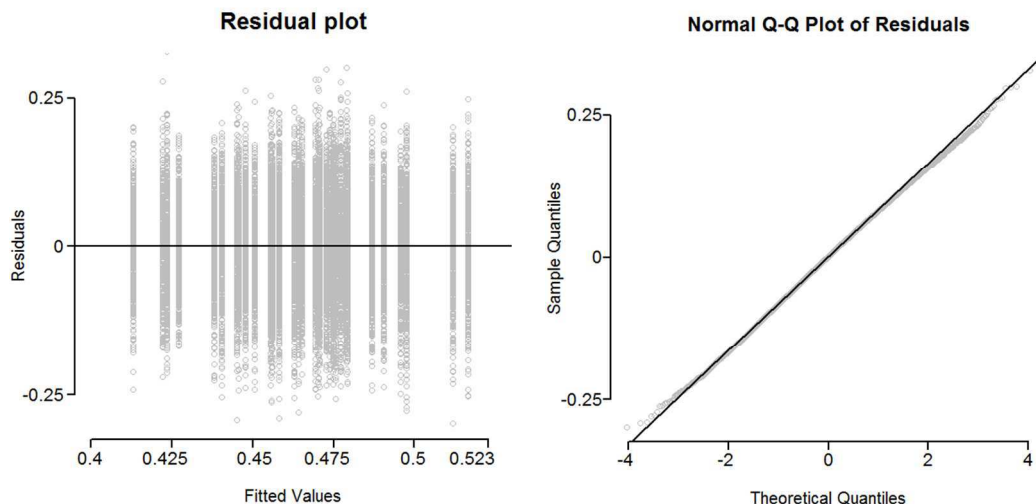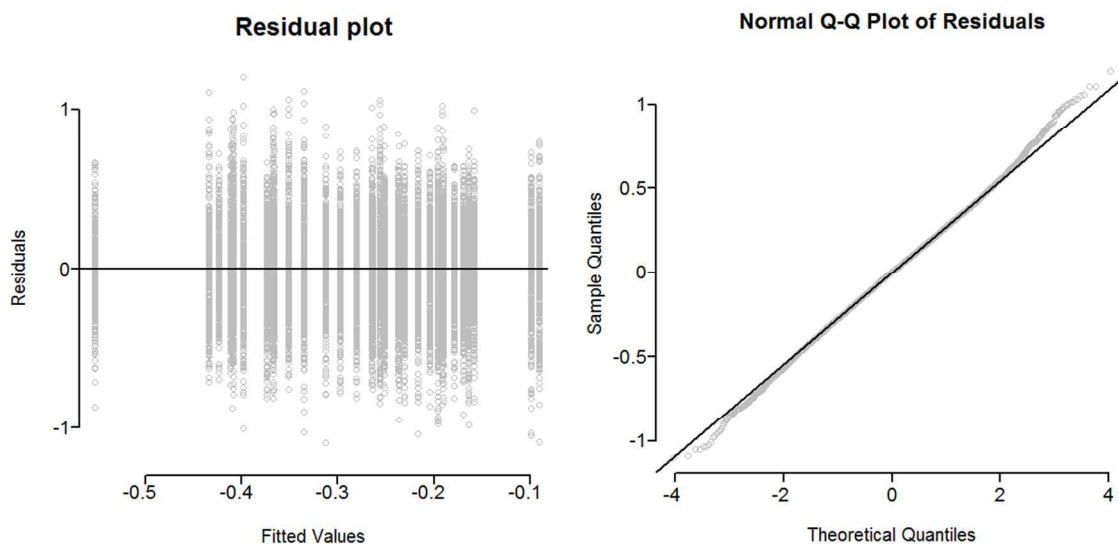
Linear Mixed Effect Model – axon diameter. The parameter estimates for the fixed effects model of *axon diameter*, including condition, region and their interaction, are shown in Table S2. In this model, a log transformation is applied to axon diameter to normalize the data.

Table S2: LME for log(axon diameter)

Random Effects	Standard Error		
Mouse (Intercept)	0.0586		
Mouse (Region - LOTl)	0.0655		
Mouse (Region - LOTm)	0.0997		
Residual	0.2781		
Fixed Effects	**Level**	**Estimate**	**Standard Error**
Intercept		-0.4060	0.0242
Condition	CSR (reference)	0	0
	SD	0.0691	0.0308
	RS	0.0045	0.0275
	S	0.0019	0.0257
Region	CC (reference)	0	0
	LOTl	0.1660	0.0196
	LOTm	0.1675	0.0292

Residual plots (shown below) were used to assess the model assumptions of normality and constant variance. From the scatter plot of residuals vs. fitted values and the qq-plot, we found no evidence against either of the assumptions.
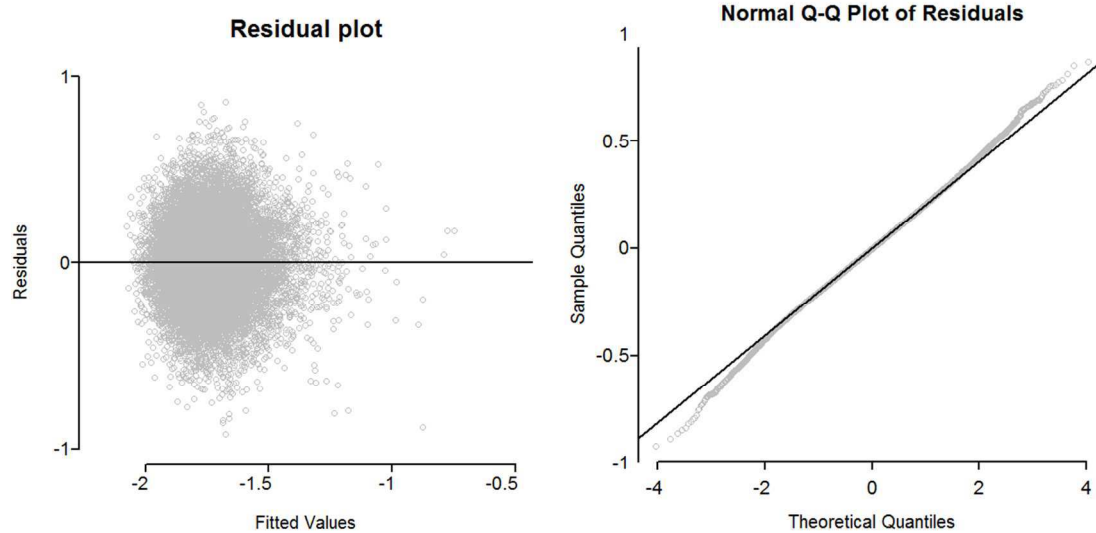

Linear Mixed Effect Model – myelin thickness. Table S3 shows the parameter estimates for the fixed effects model of *myelin thickness*, including condition, region and their interaction. In this model, a log transformation is applied to *myelin thickness* to normalize the data.

Table S3: LME for log(myelin thickness)

Random Effects	Standard Error		
Mouse (Intercept)	0.0798		
Mouse (Region – LOTl)	0.1250		
Mouse (Region – LOTm)	0.0928		
Mouse (axon)	0.1061		
Mouse (axon * LOTl)	0.1193		
Mouse (axon * LOTm)	0.0996		
Residual	0.2104		
Fixed Effects	**Level**	**Estimate**	**Standard Error**
Intercept		-2.1906	0.0324
Condition	CSR (reference)	0	0
	SD	0.0398	0.0379
	RS	0.0349	0.0339
	S	0.0334	0.0318
Region	CC (reference)	0	0
	LOTl	0.1892	0.0444
	LOTm	0.0995	0.0393
Axon Diameter	-	0.5426	0.0333
Condition by Region Interaction	CSR, CC (reference)	0	0
	SD, LOTl	0.0062	0.0392
	SD by LOTm	0.0103	0.0450
	RS, LOTl	-0.0893	0.0356
	RS, LOTm	0.0769	0.0414
	S, LOTl	0.0264	0.0337
	S, LOTm	0.0934	0.0385
Region by Axon Interaction	CC (reference)	0	0
	LOTl	-0.1671	0.0388
	LOTm	-0.2325	0.0338

Residual plots (shown below) were used to assess the model assumptions of normality and constant variance. From the scatter plot of residuals vs. fitted values, we found no evidence against the constant variance assumption. The qq-plot shows that the tails of the residuals are heavier than a normal distribution, however the LME analysis is robust to such minor departures from normality[1].

Residual plot

**Normal Q-Q Plot of Residuals**

Linear Mixed Effect Model – axonal density. Table S5 shows the parameter estimates for the fixed effects model of *axonal density*, including condition, region and their interaction. In this model, a log transformation is applied to *axonal density* to normalize the data.

Table S5: LME for log(axonal density)

Random Effects	Standard Error		
Mouse (Intercept)	0.0470		
Residual	0.1843		
Fixed Effects	**Level**	**Estimate**	**Standard Error**
Intercept		-0.8924	0.0428
Condition	CSR (reference)	0	0
	SD	0.0001	0.0611
	RS	-0.1075	0.0549
	S	0.0303	0.0508
Region	CC (reference)	0	0
	LOTl	0.2187	0.0333
	LOTm	-0.1288	0.0335

Residual plots (shown below) were used to assess the model assumptions of normality and constant variance. From the scatter plot of residuals vs. fitted values and the qq-plot, we found no evidence against the assumptions.
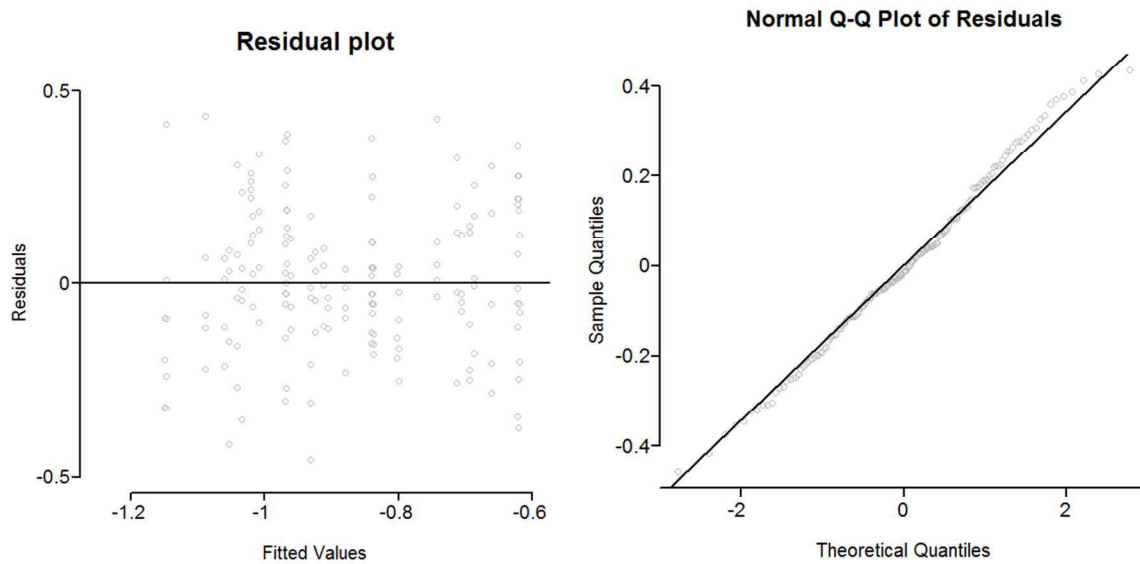
Linear Mixed Effect Model – intermodal distance. The parameter estimates for the fixed effects model of *internodal distance,* including only condition as a fixed effect (Table S6).

Table S6: LME for intermodal distance

Random Effects	Standard Error		
Mouse (Intercept)	6.873		
Residual	48.031		
Fixed Effects	**Level**	**Estimate**	**Standard Error**
Intercept		200.3068	3.7498
Condition	CSR (reference)	0	0
	SD	-9.1578	6.2212
	S	0.8543	6.2620

Residual plots (shown below) were used to assess the model assumptions of normality and constant variance. From the scatter plot of residuals vs. fitted values and the qq-plot, we found no evidence against either assumption.
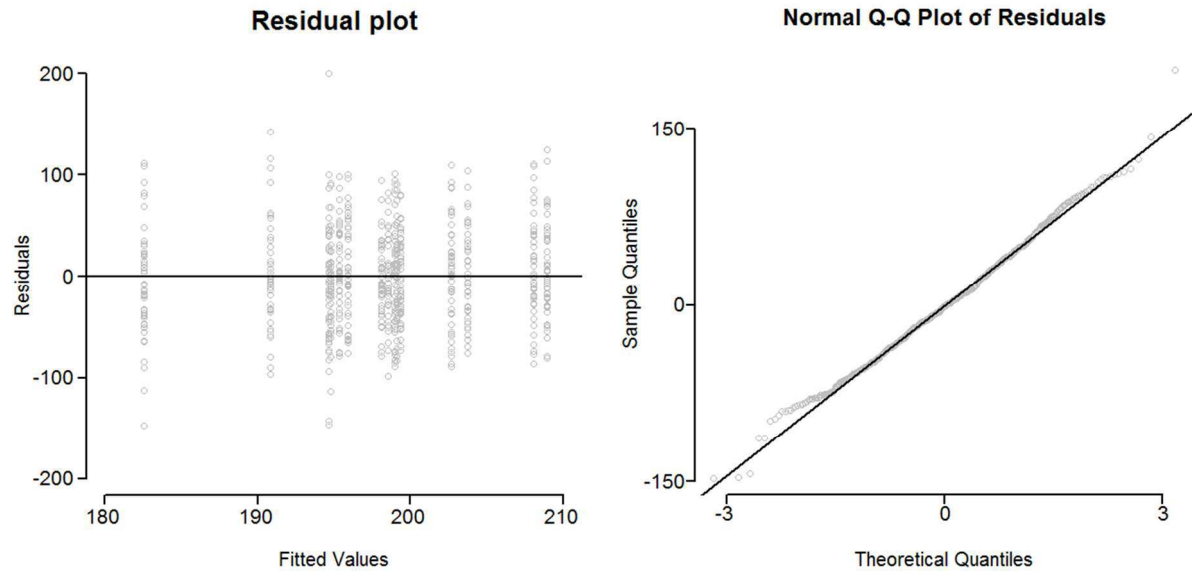
Residual plot

Normal Q-Q Plot of Residuals

Linear Model – corticosterone. The parameter estimates for the fixed effects model of *corticosterone*, including only condition as a fixed effect (Table S7).

Table S7: LM for (corticosterone) ^ (1/2)

Fixed Effects	Level	Estimate	Standard Error
Intercept		11.479	1.122
Condition	CSR (reference)	0	0
	SD-H	1.126	1.586
	SD-O	1.271	1.664
	RS	-2.594	1.664
	S	-4.123	1.664

A square root transformation was applied to stabilize the residual variance. Residual plots (shown below) were used to assess the model assumptions of normality and constant variance. From the scatter plot of residuals vs. fitted values and the qq-plot, we found no evidence against either assumption.
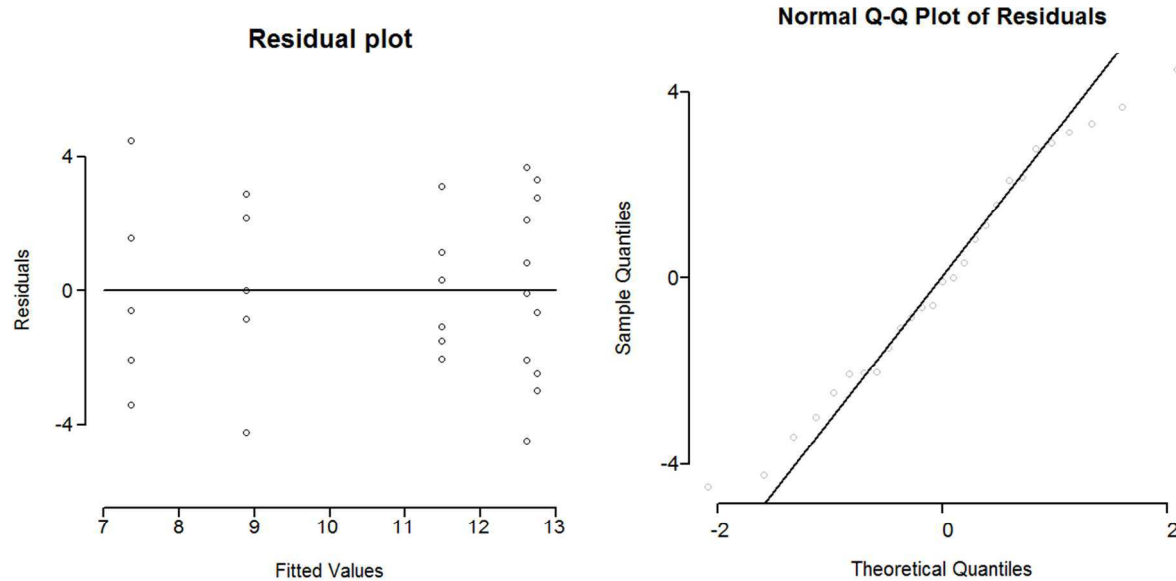
Residual plot

Normal Q-Q Plot of Residuals

Repeated Measures ANOVA

An additional validation of the results was performed using a more traditional repeated measures ANOVA analysis. We first calculated the average response variable (g-ratio, myelin thickness, axon diameter) in each brain region, for each mouse. This resulted in 3 (repeated) observations for each mouse, one for each brain region. A repeated measures ANOVA was then applied with *condition* as a 4-level between subjects factor (S, SD, CSR, RS) and *region* as a 3-level within subjects factor (CC, LOTl, LOTl).

The result of applying the repeated measures ANOVA analysis to the g-ratio data was a trend effect of condition ($F_{3,21} = 2.386$, $p = 0.0979$) comparable to a significant effect of condition for the LME model ($p = 0.0496$). The result of applying the repeated measures ANOVA analysis to the axon diameter data was no significant effect of condition ($F_{3,21} = 1.809$, $p = 0.1764$) comparable to the non-significant effect of condition in the LME model ($p = 0.1971$). To provide a fair comparison between repeated measures ANOVA and LME analysis of myelin thickness, we performed the analyses without including axon diameter as a covariate, as there is no natural way to include axon diameter as a covariate in a repeated measures ANOVA analysis. For the analysis of myelin thickness, the repeated measures ANOVA analysis found a significant effect of condition ($F_{3,21} = 3.702$, $p = 0.0278$) comparable to a significant condition effect identified by the LME model ($p = 0.0382$; note this is different than the result in the main text which includes axon diameter as a covariate). Overall, the results obtained with the repeated measures ANOVA and LME analyses are very consistent.

References

1. Verbeke G, Lesaffre E. The effect of misspecifying the random-effects distribution in linear mixed models for longitudinal data. *Comput Stat Data Anal*. 1997;23(4):541-556. doi:10.1016/S0167-9473(96)00047-3.

Reviewer information page

Number of tables: 0

Number of figures: 4

Abstract word count: 205

Statement of Significance word count: 119

Word count: Introduction (638), Methods (2719), Results (1017), Discussion (1521).

Supplementary Material: Methods for Linear Mixed Effect Models and ANOVA analyses

Myelin modifications after chronic sleep loss in adolescent mice

Michele Bellesi[1,2]*, John Douglas Haswell[1]*, Luisa de Vivo[1], William Marshall[1], Patrick H Roseboom[1], Giulio Tononi[1], Chiara Cirelli[1].

* Co-first authors

1. Department of Psychiatry, University of Wisconsin-Madison, 6001 Research Park Blvd, Madison, WI 53719 USA
2. Department of Experimental and Clinical Medicine, Section of Neuroscience and Cell Biology, Università Politecnica delle Marche, Ancona, 60026, Italy

Corresponding authors:

Chiara Cirelli
Dept. of Psychiatry
University of Wisconsin-Madison
6001 Research Park Blvd
Madison, WI 53719
USA
ccirelli@wisc.edu phone (608) 263-9236

or

Michele Bellesi
Dept. of Experimental and Clinical Medicine, Section of Neuroscience and Cell Biology
Università Politecnica delle Marche
Via Tronto 10/A
60126, Ancona
Italy
michele.bellesi@gmail.com phone +39 071 2206050

Abbreviated title: sleep loss leads to myelin changes

Author contributions: MB: devised and performed the experiments, analyzed the data, and wrote the manuscript. DH performed the experiments, analyzed the data, and wrote the manuscript. LdV performed the experiments and carried out the acquisition of the EM images. PHR performed corticosterone analysis. WM performed statistical analysis. GT and CC devised the experiments and wrote the manuscript.

2

ABSTRACT

Study Objectives. Previous studies found that sleep loss can suppress the expression of genes implicated in myelination and can have adverse effects on oligodendrocyte precursors cells. On the other hand, sleep may favor myelination by promoting the expression of genes involved in its formation and maintenance. Albeit limited, these results suggest that sleep loss can have detrimental effects on the formation and maintenance of myelin.

Methods. Here we tested this hypothesis by evaluating ultrastructural modifications of myelin in two brain regions (corpus callosum and lateral olfactory tract) of mice exposed to different periods of sleep loss, from a few hours of sleep deprivation to ~5 days of chronic sleep restriction. In addition, we measured the internodal length - the distance between consecutive nodes of Ranvier along the axon - and plasma corticosterone levels.

Results. We find that g-ratio – the ratio of the diameter of the axon itself to the outer diameter of the myelinated fiber – increases after chronic sleep loss. This effect is mediated by a reduction in myelin thickness and is not associated with changes in the internodal length. Relative to sleep, plasma corticosterone levels increase after acute sleep deprivation, but show only a trend to increase after chronic sleep loss.

Conclusions. Chronic sleep loss may negatively affect myelin.

KEYWORDS: sleep, mice, myelin, forebrain, electron microscopy

STATEMENT OF SIGNIFICANCE

In both rodents and humans there is indirect evidence that sleep loss may be detrimental for myelin. The present study is the first to assess morphologically whether different regimes of sleep loss, from few hours to several days, can affect the ultrastructure of myelin. Using electron microscopy, more than 17000 myelinated axons in two different brain regions were evaluated to obtain a comprehensive view of the effects of sleep loss on the white matter. We found that chronic sleep loss can reduce myelin thickness, an effect that may have important functional consequences given the fundamental role of myelin in optimizing the information flow throughout the brain. These results suggest that sleep may be important in maintaining a healthy myelin.

INTRODUCTION

Myelin is a substance rich in lipids and proteins that wraps around nerve fibers. It is produced by oligodendrocytes and its function is to protect and insulate the axons and enhance the transmission speed of electrical impulses [1]. Optimal speed of neural transmission is crucial for the successful integration of information across distant brain regions.

Sleep is a tightly regulated phenomenon. A sleep deficit causes a compensatory increase in the intensity and duration of sleep, whereas excessive sleep reduces sleep propensity [2]. Many lines of evidence have also shown that lack of sleep leads unavoidably to negative consequences [3]. At the cellular level, sleep deprivation increases metabolic demand leading to higher mitochondrial activity, which in turn can lead to mitochondrial stress and oxidative damage [4,5]. In the cerebral cortex of adolescent mice, sleep loss is associated with increased cytoplasmic area occupied by mitochondria, presence of extra-large mitochondria, signs of lysosomal activation, and deposition of lipofuscin granules [6]. Moreover, lack of sleep triggers the unfolded protein response, which can slow down the synthesis of most proteins [7]. Finally, wake is associated with overall high neuronal activity combined with lower clearance of solutes from the interstitial space [8], which can lead to higher extracellular glutamate levels [9,10] and increased risk for excitotoxicity. Little is known, however, about the specific effects of sleep deprivation on myelin.

Recent transcriptomic analysis performed on oligodendrocyte-enriched samples of mouse forebrain showed that the expression of hundreds of transcripts ready to be translated into proteins changes because of sleep and wake [11]. Many genes implicated in apoptosis and cellular stress (*Acin1*, *Bcat1*, *Otud7b*, *Nr4a1*, *Hip1*, *Irf8*, *Traf6*, *HSPE1*, and *HSP90aa1*) were upregulated during spontaneous wake and short (~4h) sleep deprivation relative to baseline

sleep. In contrast, a number of genes involved in lipid metabolism and in particular in glycerophospholipid biosynthesis - *Dgat2*, *Cds1*, *Elovl7*, *Chka* – as well as in myelination - *Opalin*, *Pllp*, *Qk* - were transcribed preferentially during sleep [11]. Opalin is thought to be important for myelin stabilization at the paranodal site [12] while Plasmolipin participates in the biogenesis of myelin by forming membrane domains at the Golgi level [13]. *Qk* regulates several myelin related-transcripts (i.e. *Mbp*, *Mag*) at the post-transcriptional level by modulating their mRNA stability and distribution [14]. Consequently, mice lacking *Qk* (quaking viable mice) display a remarkable deficit of compact myelin [14].

In humans, a single night of sleep deprivation can induce widespread changes in diffusion tensor imaging (DTI) indices of white matter microstructure [15]. Moreover, a recent structural MRI study showed that white matter tracts of limbic and sensorimotor regions, mainly in the right side, displayed low values of Fractional Anisotropy (FA) in patients with primary insomnia [16]. Another recent structural MRI study carried-out in 448 community-dwelling older adults showed that poor sleep quality was associated with reduced global fractional anisotropy and increased global axial diffusivity and radial diffusivity values of white matter tracts, suggesting that the white matter may be especially sensitive to sleep loss [17]. These studies, however, lack the spatial resolution to identify the exact microanatomical substrates affected by lack of sleep, leaving unanswered the question whether extended wake can have specific detrimental effects on the formation and maintenance of myelin. Experiments in animals showed, for instance, that modifications of the fractional anisotropy of water diffusion, which is the basis for DTI, can also be related to changes in axon diameter or axon packing density[18].

Here we addressed this question by evaluating ultrastructural modifications of myelin in mice exposed to different regimes of sleep loss, from a few hours of sleep deprivation to ~5 days of

chronic sleep restriction. We find that the ratio between the diameter of the axon itself to the

outer diameter of the myelinated fiber (g-ratio), increases after chronic sleep loss, and this effect

is accounted for by a decrease in myelin thickness.

7

MATERIAL AND METHODS

Animals. Four week old male homozygous B6.Cg-Tg(Thy1-YFP)16Jrs/J transgenic mice were used in this study. These mice express yellow fluorescent protein (YFP) in a subset of cortical pyramidal neurons [19] and have been studied extensively to assess the link between sleep and synaptic plasticity during development [20–22]. All animal procedures followed the National Institutes of Health Guide for the Care and Use of Laboratory Animals and facilities were reviewed and approved by the IACUC of the University of Wisconsin-Madison, and were inspected and accredited by AAALAC.

Experimental groups. Mice were housed in environmentally controlled recording chambers with free access to food and water (12 h:12 h light-dark cycle; lights on at 08:00). They were divided in four experimental groups (Figure 1A): sleeping (S) mice (n=8) were sacrificed during the light phase after 6–8 h of undisturbed sleep; sleep deprived (SD) mice (n=6) were kept awake for the first 6–8 h of the day using novel objects; chronically sleep restricted (CSR) mice (n=10) were sleep restricted for 4 ½ days using a combination of methods, including exposure to novel objects and gentle handling during the day and forced locomotion on a slowly rotating treadmill during the night. The treadmill (36 cm long x 42 cm wide) was located above a tray filled with 2-3 cm of water, and the movement speed (~1.5 cm/sec) was low enough that mice could easily avoid falling into the water if they moved continuously. Video cameras and/or direct visual observation were used to constantly monitor the mice while on the platform. In previous experiments, we found that this method decreases overall sleep duration by ~ 70% [6]; recovery sleep (RS) mice (n=3) were allowed to rest undisturbed for ~32 h after CSR. In the current study, SD and CSR mice were under constant and direct visual observation by one or more experimenters. By contrast, the sleep/wake behavior of S and RS mice was assessed using

8

motion detection monitored with infrared video cameras, to avoid disturbing the mice. As in

previous studies [20,23] behavior was quantified online at 1-sec time resolution, thus allowing us to

kill the mice after a period of well consolidated sleep (>45 min, interrupted by periods of wake

of 4 min). All mice were sacrificed between 14:40 and 18:00 to maintain the time of brain

collection within the same 3-h circadian window for all experimental groups (Figure 1A).

Subsets of animals in each experimental group were used for electron microscopy and/or

confocal microscopy experiments (see below).

Electron Microscopy Experiments. S (n=4), SD (n=2), CSR (n=3), and RS (n=3) mice were

anesthetized with isoflurane (3% volume to oxygen), then transcardially perfused for 30 seconds

with normal saline (0.9%, 41°C) followed by 10 minutes of 2.5% glutaraldehyde and 4%

paraformaldehyde dissolved in 0.1M sodium cacodylate buffer (pH 7.4, 41°C). The percentage

of time spent asleep in the last 6h before the perfusion was $75.5 \pm 3.5\%$ in S mice, and $64.1 \pm$

7.8% in RS mice. Brains were then collected and post-fixed in the same fixative solution

overnight at 4°C. It is worth noting that, although fixation has strong impact on ultrastructure, all

the mice received similar amount of fixative and all samples were processed in parallel.

Therefore, it is highly unlikely that the fixation and staining procedure biased the results.

Coronal 120 μm sections were sectioned using a vibratome, and then stored in cryoprotectant

solution at -20°C. Sections at the level of the decussation of the Anterior Commissure (+0.14

mm A/P from Bregma) were used. Two circular samples ~1mm in diameter were punched out

from the sections for each animal. The first sample was aimed at the corpus callosum (CC)

superficial to the lateral ventricle (Figure 1B-D). This cut was positioned so that the sample

included, in the dorso-ventral direction, both the grey matter above the cingulum of the CC and

the lateral ventricle beneath the CC. Medio-laterally, it spanned the entirety of the lateral

ventricle, including the lateral septal nucleus and the caudate-putamen on its borders. The second

sample was positioned to include the entirety of the lateral olfactory tract (LOT; Figure 1E-G).

All staining was performed at room temperature (RT) with agitation unless otherwise stated.

Sections were first rinsed in cacodylate buffer and stained in 1% potassium ferrocyanide/2%

osmium tetroxide for 1 hour on ice and in the dark, with no agitation. Next, sections were rinsed

in cacodylate buffer, stained in 1% thiocarbohydrazide for 20 min, rinsed in H_2O and stained in

2% osmium tetroxide for 30 minutes at RT, in the dark with no agitation. Sections were then

rinsed in H_2O, stained with 1% uranyl acetate at RT for 2 hours with no agitation, then overnight

at 4°C. The next day the sections were rinsed in H_2O and then stained in lead aspartate for 30

minutes (pH 5.5, 60°C), followed by rinses in in H_2O and dehydration through a series

of increasing alcohol concentrations (35%, 50%, 70%, 80%, 90%, 95%, 100%), and then

propylene oxide. Dehydrating solutions were kept chilled in ice. Sections were infiltrated

through a series of increasing concentrations of Durcupan ACM resin in propylene oxide (25%,

50%, 75%; 2 hours each concentration), and then overnight in 100% Durcupan. The following

day, sections were moved to a newly prepared 100% Durcupan solution for an additional 8

hours. Sections were then embedded in ACLAR embedding film and heated in an oven for 2

days at 60°C. Excess ACLAR was cut away from the embedded sample under a

stereomicroscope, resulting in blocks of approximately 1 mm^2. The block was attached to the top

surface of an aluminum pin using a conductive silver epoxy as an adhesive. The silver epoxy was

then polymerized by placing the samples in a 60°C oven overnight. The following day, excess

ACLAR and tissue were trimmed away from the sample under a stereomicroscope.

Imaging. Samples were imaged in a ΣIGMA VP field emission scanning electron microscope

with the following parameters: aperture 30μm; acceleration voltage 1.8 kV; ~3nm per pixel,

12000 × 12000 pixels per image. Within the CC immediately superficial to the lateral ventricle, the axons were horizontally oriented while above, a layer of myelinated axons oriented orthogonally to the coronal plane was present (Figure 1B-D). These orthogonally oriented myelinated axons were densely grouped on the medial portion of CC above the ventricle, and were relatively sparse above the cingulum, interspersed with radially oriented unmyelinated axons. Because the medial portion had dense myelination and a visually distinct border between the white matter tract and surrounding grey matter, this region (i.e. the medial portion of CC superficial to the lateral ventricle) was selected for imaging and analysis. Contrary to the CC, the LOT sample did not have easily defined landmarks. However, at this level (+0.14 mm A/P from Bregma) the tract has the shape of a teardrop, with a wider ventromedial portion and a thinner dorsolateral portion. While the orientation of myelinated axons varies across the LOT, with both orthogonal and obliquely oriented axons, there was no clear grouping of these differently oriented axons, and no consistent patterns across animals. Since axons on the surface of the LOT are newer, as axons are added superficially [24], we divided the tract into two sections, one located more dorsally and laterally (lateral LOT, LOTl) and the grey-matter apposing region of the LOT, located more medially (medial LOT, LOTm), both vertically spanning throughout the LOT.

Image analysis. The g-ratio is defined as the ratio of the axonal segment diameter to the total fiber segment diameter and was measured by tracing two components of the axonal fiber, the axonal segment containing the cytoplasm and membrane of the myelinated axon, and the fiber segment that includes both the axon and its surrounding myelin. The axonal segment is defined as the area contained within a selection drawn on the outer limit of the axonal membrane. The fiber segment is defined as the area contained within a selection drawn on the outer limit of the surrounding myelin. Given the dense apposition of myelinated axons, in some cases it was

difficult to determine where the outer limit of one myelin sheath ended, and the outer limit of an adjacently apposed sheath began. Thus, a straight line was assumed to bisect the two apposed sheaths from the vertices formed by their apposition. In addition to the g-ratio, the axonal segment diameter and the myelin thickness (fiber segment diameter minus axonal segment diameter)/2 were measured. Multiple images spanning an area of ~4000 μm^2 were used to calculate the myelinated axon density (N of myelinated axons per μm^2) for each area used for g-ratio calculation.

Confocal experiments. S (n=4), SD (n=4), and CSR (n=7) mice were anesthetized with isoflurane (3% volume to oxygen) and transcardially perfused for 30 seconds at RT with normal saline (0.9%), followed by 8 minutes of 4°C 4% paraformaldehyde (PFA) in 0.1M phosphate buffer. In S mice, the percentage of time spent asleep in the last 6h before the perfusion was 83.6 ± 8.7%. Brains were then extracted and post-fixed in the same fixative solution overnight at 4°C. Coronal sections 50μm thick were obtained using a vibratome, and stored in 0.05 M phosphate buffered saline (PBS) with 0.5% sodium azide at 4°C.

Immunohistochemistry. Sections (between +0.1 and 0.14 mm A/P from Bregma) were used for immunohistochemistry. All steps were performed at RT with agitation unless otherwise stated. Sections were rinsed in 0.5 M PBS (3 x 5 min) to remove residual PFA and sodium azide and then placed in blocking solution containing 5% normal goat serum, 0.3% TritonX for 1.5 hours. Sections were incubated in a primary antibody solution of mouse anti-CASPR (1:1000 parts to water; abcam, ab105571) overnight without agitation, rinsed in PBS (3 x 5 min), and then incubated in a secondary antibody solution of Alexa Fluor 568 goat anti-mouse IgG (1:500 parts to water; Invitrogen, a11004) overnight without agitation. As shown in pilot tests, the long incubation with the secondary antibody at RT was necessary to stain throughout the white matter

of the 50 μm thick sections. Sections were then rinsed in 0.5M PBS (3 x 5 min), mounted to a glass slide, air dried, and secured with a coverslip with Vectashield mounting medium (H-1000, Vector). Because the structures of interest (axons within the white matter tracts) are very large and the sections are subject to possible mechanical distortion from pressure of the coverslip, varnish was built around the corners of the glass slide, to allow the coverslip to sit upon.

Imaging. Sections were imaged using a confocal microscope using PrairieView software and a UPlan FL N × 40 objective lens (numerical aperture 1.3). Image stacks with a resolution of 2048×2048 pixels and a 1 μm stack interval were taken across the 50 μm thick sections. The fields in which these image stacks were acquired were from the CC directly dorsal to the lateral ventricles. This area was selected because of its low density of Thy1-YFP+ axons, which permits a clearer attribution of CASPR+ paranodes to a single YFP+ fiber amongst densely clustered axons. Moreover, the axons within this area tend to run parallel to the coronal plane, which is necessary to obtain an internodal length segment in its entirety. Finally, image stacks were acquired with a ~5% overlap so that internodal lengths spanning multiple fields could be reconstructed by identifying the same landmarks between adjacent fields.

Image analysis. From the image stacks previously acquired, areas where a pair of CASPR fluorescent puncta (corresponding to a pair of paranodes surrounding the node) colocalized with a Thy1-YFP+ axon were highlighted. If two of the previously highlighted areas were connected by the same axon, the internodal length between those paranodal pairs was measured in the X-Y plane. This measurement, specifically, was taken from the internal edge of the CASPR fluorescence pair, along the Thy1-YFP axon, to the internal edge of the next CASPR fluorescence pair. The length in the Z axis was first approximated by recording the section number in the image stack for each of the paranodes (sections were 1 μm apart in the Z axis),

and then by using the distance between the two paranodes in the Z axis and the length of the internode in the X-Y plane to calculate the hypotenuse of those two components, to obtain the full measurement of the internode.

Plasma corticosterone quantification. S (n = 5), SD (n = 11), CSR (n = 6), and RS (n = 5) mice (all males) were used for this experiment. Some SD mice (n = 5) were sleep deprived for 6-8 h by exposure to novel objects (SD-O) as done for the myelin experiments, while other animals were kept awake for 6-8 h by gentle handling (SD-H; n = 6). The goal was to assess whether in our experimental conditions one type of enforced waking is more stressful than the other, since both methods were used in CSR mice. For S and RS mice the percentage of time spent asleep in the last 6h before the perfusion was 76.4 ± 6.5% and 69.5 ± 5.6%, respectively. All mice were killed by cervical dislocation and quickly decapitated. Approximately 200 μl of blood was collected from the chest cavity of each mouse, placed in a tube containing 5 μl of 40 mg/ml EDTA and centrifuged at 2,000g for 15 min at 4°C to separate the plasma. Plasma was assayed for corticosterone using the MP Biomedicals (Orangeburg, NY) ImmuChem corticosterone double antibody radioimmunoassay (RIA) kit. The samples were diluted 200-fold in assay diluent and all samples were assessed in duplicate in a single assay following manufacturer's instructions. According to the manufacturer the intra-assay and inter-assay coefficients of variation (CVs) were 7.1% and 7.2%, respectively.

Statistical analysis. Statistical analysis was performed using a linear mixed effects (LME) model that includes both random and fixed effects [25] . The general matrix form of the LME is:

$$y = Zu + X\beta + \epsilon$$

where,

$$u \sim N(0, \Sigma),$$

and

$$\epsilon \sim N(0, I\sigma^2).$$

In this model, y is the vector of response variables, either g-ratio, axon diameter, or myelin thickness, u is the vector of random effects (independent and normally distributed with mean zero and covariance Σ), and β is the vector of fixed effects in the model. Design matrices Z and X link the response variables to the random and fixed effects, and ϵ is the residual values, assumed to be independent and normally distributed with constant variance σ^2.

The use of LME models offers several advantages over traditional ANOVA methods for repeated measures experiments. One advantage is the ability to handle unbalanced data, e.g. missing or corrupted observations. In the current study, the unbalanced data is due to differing numbers of axons in each sample of brain tissue. The other benefit, highly relevant in the current study, is greater flexibility and statistical power for post-hoc comparisons. This increased power is due to the flexibility in the LME model to specify different covariance (random effects) structures. Having a correct variance structure allowed us to perform post-hoc tests from within the model, leveraging all of the data to maximize statistical power. Repeated measures ANOVA on the other hand, can only support simple variance structure, i.e. ANOVA assumes that the variance of the differences between two levels of a factor is equal for any two levels (the sphericity assumption). This assumption is problematic however, because even small departures from sphericity can inflate the error rate of post-hoc tests[26].

To select the model structure, we first used the Akaike Information Criterion (AIC), identifying the set of fixed and random effects that minimize the AIC. If the fixed effect structure contained

any interaction terms involving within-subject factors, we then expanded the random effects structure to also include these factors, as this is necessary to accurately test for the significance of such interactions[27]. Parameter estimation of LMEs was performed using numerical maximum likelihood estimators, implemented in R by the lmer() function of the lme4 package [28] . To test the significance of effects in the LME model, we used likelihood ratio tests. Post-hoc tests were performed using the glht() function of the multcomp package in R, with p-values adjusted for multiple comparisons using the single-step method [29]. Note that when compared, the two methods (LME model, repeated measures ANOVA) gave very similar results for the three main analyses performed in this study (the effect of condition on g-ratio, axon diameter and myelin thickness). Specifically, the repeated measures ANOVA analysis confirmed the primary finding of the study as reported below using LME models, i.e. a significant decrease in myelin thickness after chronic sleep restriction. Detailed results for all statistical models (LME and ANOVA) are presented in the Supplementary Material.

Values of plasma corticosterone levels were compared across groups using one-way ANOVA followed by Tukey's post-hoc test.

RESULTS

Myelin thinning occurs after chronic sleep loss

We used four groups of young male mice (Figure 1A) that were either allowed to sleep ad libitum (>6h of sleep, S mice), or were subjected to different degrees of sleep loss before brain collection: acute sleep deprivation (6-8h of wake enforced with novel objects, SD mice), chronic sleep restriction for 4½ days (CSR mice), and recovery sleep after CSR (4½ days of CSR followed by 1½ day of recovery sleep, RS mice). To assess the effects of sleep and wake on the

white matter we measured g-ratio, axon diameter, and myelin thickness of thousands of axons (S: n=5918; RS: n=4593; SD: n=3045; CSR: n=4338) in two different brain regions, the Corpus Callosum (CC, Figure 1B-D) and the Lateral Olfactory Tract, which was divided into medial and lateral sections (LOTm, LOTl, Figure 1E-G). For each of these variables we applied a Linear Mixed Effect Model (LME) model that accounts for random and fixed effects to estimate statistical significant changes among experimental conditions (see Methods). It is also worth noting that during the scoring process we never observed ultrastructural signs of demyelination for the above 17000 axons evaluated.

We first measured the g-ratio, the ratio of the inner axonal diameter to the total outer diameter, because it is a highly reliable measure of axonal myelination[30]. We found evidence of a condition effect ($\chi2 = 7.83$, df = 3, p-value = 0.0496). Specifically, we observed that CSR mice generally had the largest g-ratio, while S animals generally had the lowest g-ratio, and SD/RS animals had intermediate values. Post-hoc tests between conditions (corrected for multiple comparisons) confirmed these observations, revealing a significant difference between the two most "extreme" conditions, CSR and S (z = 3.205, p = 0.0075, 2.0% decrease), while RS and SD mice showed no significant differences relative to any of the other groups (Figure 2A).

For axonal diameter, we found that SD mice generally had the largest axon diameter (see Figure 2B), but the effect of condition was not significant ($\chi2 = 4.676$, df = 3, p-value = 0.1971). Conversely, for myelin thickness, we found a condition by region interaction ($\chi2 = 20.149$, df = 6, p-value = 0.0026). Specifically, CSR mice generally had the smallest myelin thickness across brain regions with the exception of LOTl, in which myelin thickness was smallest in RS mice. There was no obvious and consistent ordering among the remaining conditions. Post-hoc tests between conditions (corrected for multiple comparisons) confirmed that myelin thickness in CSR

mice was significantly lower than in S animals (z = 4.559, p = 0.00004, 7.6% decrease) and trended to be lower than in SD animals (z = 2.374, p = 0.0812, 4.6% decrease), but did not differ between CSR and RS animals (z = 1.813, p = 0.2656, 3.1% decrease). Myelin thickness was also significantly lower in RS animals than in S animals (z = 2.685, p = 0.0362, 4.3% decrease), while no other significant differences were found across conditions (Figure 2C-D). To investigate whether the effect of CSR on myelin thickness varies based on axon diameter, we incorporated a co-variate (axon diameter) in the model structure, finding no significant interaction between the effect of condition and axon diameter ($\chi2$ = 3.799, df = 3, p-value = 0.2839; Figure 2E).

Overall, these results indicate that the g-ratio increases after chronic sleep loss, and this result is explained by a reduction in myelin thickness rather than by an increase in axon diameter. Moreover, the effect of chronic sleep loss on myelin thickness is seen in all axons, independent of their size, and does not seem to recover with 32h of recovery sleep.

The density of myelinated axons is not affected by sleep loss

Next, we quantified the density of myelinated axons in the same images used for the analysis of the g-ratio in CC and LOTs regions of S, RS, SD, and CSR mice. We found no significant difference in the density of myelinated axons across the experimental conditions ($\chi2$ = 6.075, df = 3, p-value = 0.108) (Figure 3A). However, we found that the density of myelinated axons varied across regions, being lowest in LOTm, highest in LOTl and intermediate in CC (Figure 3B).

Internodal length is not affected by sleep loss

Myelin thickness is linearly correlated with the internodal length [31], i.e. the distance between consecutive nodes of Ranvier along the axon. Given the changes of myelin thickness in SD and S mice relative to CSR mice, we tested whether these modifications were associated with changes in intermodal length. Using immunostaining against CASPR, a protein highly expressed at paranodal sites, we highlighted nodes along YFP+ axons and measured the internodal distances in a subset of CC axons of independent groups of S, SD, and CSR mice (S: 173 internodes; SD: 180 internodes; CSR: 316 internodes; Figure 3C). Using again an LME model, we found no evidence of a condition effect (χ^2 = 2.446, df = 2, p-value = 0.294, Figure 3D), indicating that internodal length did not differ across experimental groups.

Plasma corticosterone levels increase after sleep loss

To determine whether the effects of sleep loss on myelin could be accounted for by increased levels of stress hormones we measured plasma corticosterone levels in additional groups of S, SD, CSR and RS male mice not previously used for ultrastructural experiments. SD mice included two groups, one kept awake using novel objects (SD-O) as previously done to study myelin changes, and another exposed to gentle handling (SD-H), since both types of stimuli were used in CSR mice. Plasma levels of corticosterone changed across groups (ANOVA: $F_{4,22}$ = 3.94; p = 0.015). Specifically, they were higher in both SD-O and SD-H mice relative to S mice (both p = 0.03), whereas CSR animals did not differ from S (p = 0.13), SD-O (p = 0.94), SD-H (p = 0.95), and RS mice (p = 0.54; Figure 4). Corticosterone levels were similarly elevated with the two methods of acute sleep deprivation (SD-O vs. SD-H, p = 0.99), and were comparable after baseline and recovery sleep (S vs. RS, p = 0.90; Figure 4).

19

DISCUSSION

We assessed the ultrastructural changes of myelinated fibers in two brain regions of adolescent mice after sleep, acute total sleep deprivation, chronic sleep restriction, and recovery sleep after chronic sleep restriction. We found that in both regions chronic sleep loss is associated with thinner myelin sheaths. This effect is not associated with changes in the number of myelinated axons, and occurs in axons of all sizes. Optimal g-ratio and myelin thickness are strictly linked to conduction velocity [30,32]. Even small deviations from the optimal values can lead to delays in the propagation of nerve pulses, impacting the frequency, propagation and coupling of neural network oscillations, which are crucial for complex information processing [33]. Thus, these results suggest that possible detrimental effects of sleep loss on myelin cannot be ruled out at this stage.

To our knowledge, this the first structural evidence that loss of sleep can induce changes in myelin. Previously, molecular studies showed that long-term sleep deprivation down-regulates the expression of two myelin-related genes, one coding for Plasmolipin (*Pllp*) and the other for CD9, a membrane protein normally expressed in the mature myelin sheath [34]. More recent studies were also in line with a role of sleep in promoting myelination by showing that several genes specifically involved in myelin production and maintenance (*Qk*, *Pllp*, and *Opalin*) are preferably transcribed after a few hours of spontaneous sleep [11,35]. In light of the current results, these findings suggest that loss of sleep could lead to myelin thinning by interfering with the expression of some of the genes implicated in the myelination process.

Myelin maintenance and turnover are energetically costly processes [36], Thus, one potential mechanism to explain myelin thinning after sleep loss is that oligodendrocytes prioritize some cellular functions at the expense of others in conditions of high metabolic

20

demands, like during periods of extended wake. Converging evidence indicates that one crucial function of oligodendrocytes is to sustain axonal energy demands, likely through mechanisms that involve oligodendrocyte glycolysis, lactate production and shuttling to the axons [37–39]. In this respect, attention has been given to the lactate transporter MCT1, which excretes lactate outside the cell [38] and is highly expressed in oligodendrocytes [40]. Knocking-down its expression by 50% caused a late-onset axonal degeneration, indicating that lactate release from oligodendrocytes is indeed crucial for axonal integrity [38]. Extracellular lactate levels are low during sleep and rise during wake [41] indicating increased demand for lactate during behavioral states that show higher metabolism. However, it is currently unknown whether extracellular lactate levels remain elevated during prolonged sleep loss, and, notably, *Slc16a1,* the gene coding for MCT1, is upregulated in oligodendrocyte-enriched samples of sleeping mice [11], suggesting that lactate efflux from oligodendrocytes to axons might preferably occur during sleep.

Our results suggest that the effect of sleep loss on myelin becomes morphologically visible only after several days of sleep restriction. Acute sleep deprivation for 6-8 hours did not affect myelin structure, even if molecular studies have shown that the expression of several genes involved in myelin production is reduced with a few hours of wake [11]. In addition, we found that myelin thickness does not renormalize after ~32h of recovery sleep, suggesting that myelin changes take time both to develop and to resolve. Recent findings show that myelin is highly plastic, as its structure is affected by changes in neuronal activity [42], learning [43], or social isolation [44]. However, it is still matter of debate whether hours, days, or longer periods are needed for myelin to remodel. Relative to controls, rats trained in the Morris water maze for 5 days showed signs of white matter modifications as detected by MRI, and elevated levels of myelin basic protein (MBP) at the histological examination [45]. Another study found increased

Fractional Isotropy (FA), an MRI measure that evaluates the degree of restricted diffusion of protons in one orientation in the tissue, in the subcortical white matter of mice after 11 days of motor training, together with increased MBP expression in the same brain region [46]. However, since none of these studies used electron microscopy it is difficult to say whether the increased MBP expression was due to increased myelin thickness or increased number of axons that had become myelinated. Finally, a recent study performed in both rats and humans observed white matter structural changes in the hippocampal fornix only 2 hours after training [47], suggesting that modifications of myelin can occur more quickly than previously thought. This is in line with recent evidence showing increased FA in the white matter of human subjects after 14 hours of wake [15].

In this study, chronic sleep restriction was achieved by using a combination of methods ranging from the exposure to novel objects and gentle handling during the light phase to forced locomotion during the dark phase. Previous studies using EEG implanted mice demonstrated that this procedure can reduce total sleep time by ~ 70% [6]. Since sleep is highly regulated, any attempt to enforce sustained wake leads to "stress", that is, to a complex physiological response to re-establish homeostasis. Thus, the stress associated with our CSR method and, in fact, with any method used to enforce sustained wake, could at least partly account for the effects on myelin. There is evidence showing that chronic stress may affect oligodendrocyte physiology. For example, three weeks of repeated water immersion and restraint stress in mice led to structural modifications of the oligodendrocytes in the corpus callosum, including thicker processes and increased branching of the oligodendrocytes. These morphological changes were associated with an augmented packing of the myelinated fibers as revealed by electron microscopy analysis. However, no significant changes in myelin thickness were observed

following chronic stress[48]. In another study, the same stress procedure confirmed the lack of the effect on g-ratio, but found a 20% reduction of the node and paranodal lengths, thus suggesting that chronic stress may alter the structural organization of the node of Ranvier[49]. Furthermore, a recent study found that four weeks of chronic variable stress in mice reduced the transcription of myelin related genes (e.g. *Mag, Mobp*) in medial prefrontal cortex and nucleus accumbens, whereas it increased both *Mog* and *Mbp* expression in the corpus callosum[50]. Collectively, these results indicate that the response of oligodendrocytes to stressful experiences is complex, region dependent, and not necessarily associated with a reduction in myelin thickness.

Classical stress responses are associated with increased levels of cortisol and/or catecholamines, and there is some indication that high levels of cortisol can have a negative impact on myelination. Administration of corticosteroids during development can delay myelination [51,52], whereas early adrenalectomy increases myelination in the rat brain[53], although the evidence is not always consistent[54]. Yet, while chronic sleep loss (2 weeks) in rats consistently led to sustained activation of the sympathetic nervous system and increased release of noradrenaline thorough the brain and the body, it decreased costicosterone levels [55], and 6 nights of sleep restriction in humans did not affect serial 24-h plasma cortisol levels compared with baseline [56]. In rats, short periods of sleep restriction (4h per day) repeated for 8 days increased plasma corticosterone levels [57], but the increase was rather small as compared to the increases caused by other stressors such as restrain [57,58]. We found that acute sleep deprivation using exposure to novel objects significantly increased plasma corticosterone levels relative to sleep. By contrast, the levels of corticosterone in CSR mice were no longer significantly different from S mice, although a trend to be higher was present, and did not differ from those in SD mice, consistent with evidence that the hypothalamic–pituitary–adrenal axis of mice habituates to

repeated stress[59,60]. On one hand, these results may suggest that it is unlikely that the effects of sleep loss on myelin can be fully accounted for by increased plasma corticosterone levels, because the temporal profile of the changes in corticosterone levels poorly correlates with the modifications in myelin content. Specifically, acute sleep deprivation robustly increased plasma corticosterone levels, but myelin thickness was not affected at this point. Moreover, at the end of CSR plasma corticosterone levels were no longer significantly higher than after several hours of sleep, while myelin thickness showed a significant reduction. Finally, after 32h of recovery sleep plasma corticosterone levels did not differ from those after baseline sleep, whereas myelin thickness was still significantly smaller. On the other hand, however, it may be that even relatively mild increases in plasma corticosterone levels, when protracted, can lead to myelin changes, and the latter take time to develop and to resolve. Interestingly, the effects of high levels of noradrenaline on myelin are poorly characterized, but a few studies described a protective role of noradrenaline in experimental autoimmune encephalomyelitis, a rodent model of Multiple Sclerosis where myelin is severely impaired [61,62]. Therefore, we cannot rule out that other stress-induced changes, including increased noradrenaline levels, may play a role in the myelin thinning described in the present study.

Previous studies found that axonal diameter, myelin thickness (number of lamellae), and internodal length, i.e. the distance between two consecutive nodes of Ranvier, are linearly correlated [63,64]: axonal segments that show the largest diameter and the highest number of lamellae also display the longest internodal lengths. Although this linear relation does not hold very well for very small and very large fibers [31], it implies that changes in myelin thickness could lead to modifications of internodal length. However, despite changes in g-ratio and myelin thickness after chronic sleep loss, we found no change in internodal length, neither after short

sleep deprivation nor after chronic sleep restriction. Thus, it is possible that internodal length changes require longer time to occur or that the small myelin change that we observed (~7%) is not enough to promote a rearrangement of node positions.

Whether sleep loss can drive myelin changes in humans remains an open question. The few studies carried out so far focused on the correlation between DTI measures and sleep loss. Although they showed changes of the fractional anisotropy of water diffusion in subjects who experienced sleep loss, these measurements have several limitations and cannot resolve the microstructure of the white matter. By contrast, methods like Positron Emission Spectroscopy can use myelin specific radioligands to reveal more accurately myelin changes[65,66], and may in the future reveal more directly how poor sleep affects myelin in humans.

Disclosure Statement

FIGURE LEGENDS

Figure 1. A. Experimental design (P, postnatal day). S (sleep), SD (acute sleep deprivation), CSR (chronic sleep restriction), RS (recovery after CSR). Red arrows indicate the time of perfusion. **B.** Coronal section of Corpus Callosum (CC). **C-D.** Region of interest (**C**) selected for the analysis. Note that fibers are almost all orthogonal in this region of CC, whereas the opposite is true for the region underneath (**D**), where most of the fibers are parallel. **E.** Section of the Lateral Olfactory Tract (LOT). Medial and lateral regions are separated by a red dashed line. **F-G.** Medial (**F**) and lateral (**G**) LOT regions of interest selected for the analysis.

Figure 2. Myelin thinning occurs after chronic sleep loss**. A-C.** Distribution of g-ratio (**A**), axon diameter (**B**), and myelin thickness (**C**) measurements for S (3 mice, 5918 axons), RS (3 mice, 4593 axons), SD (2 mice, 3045 axons), and CSR (3 mice, 4338 axons). For axon diameter and myelin thickness, a log transformation has been applied to raw values, so the units are log(μm). **D.** Myelin thickness by region interaction showing that the effect of sleep loss on myelin thickness varies depending on the region. **E.** Graph showing the effect of axon diameter on myelin thickness for each of the different sleep conditions, including linear regression of myelin thickness on axon diameter (bold lines) and individual observations (dots). Note that the axes in panels A, C and D are not zeroed.

Figure 3. Sleep loss effects on density of myelinated axons and internodal length. **A-B.** Statistical analysis showing the distribution of axonal densities (**A**) for S (3 mice, 63 images), RS (3 mice, 43 images), SD (2 mice, 30 images), and CSR (3 mice, 45 images) mice and the region

26

effect (**B**). **C.** Top. Representative Corpus Callosum (CC) coronal section depicting YFP+ fibers (blue) and CASPR+ puncta (yellow). Arrowheads indicate examples of nodes considered for the analysis, which are shown at larger magnification in the squared boxes. The red line along the axon indicates the internodal length. Bottom. Scheme of representative nodes of Ranvier with paranodal sites (yellow) and the red line representing the internodal length. **D.** Distribution of internodal lengths for S (4 mice, 173 internodes), SD (4 mice, 180 internodes), and CSR (7 mice, 316 internodes) mice. Note that the axes in panels A and B are not zeroed.

Figure 4. Plasma corticosterone levels across the experimental conditions in male mice. Acute sleep deprivation for this experiment was carried out using exposure to novel objects (SD-O) or gentle handling (SD-H).

REFERENCES

1. Baumann N, Pham-Dinh D. Biology of oligodendrocyte and myelin in the mammalian central nervous system. *Physiol Rev*. 2001;81(2):871-927.

2. Borbély AA, Daan S, Wirz-Justice A, Deboer T. The two-process model of sleep regulation: a reappraisal. *J Sleep Res*. 2016;25(2):131-143. doi:10.1111/jsr.12371.

3. Cirelli C, Tononi G. Is Sleep Essential? *PLoS Biol*. 2008;6(8):e216. doi:10.1371/journal.pbio.0060216.

4. Cirelli C. Cellular consequences of sleep deprivation in the brain. *Sleep Med Rev*. 2006;10(5):307-321. doi:10.1016/j.smrv.2006.04.001.

5. Zhang J, Zhu Y, Zhan G, et al. Extended Wakefulness: Compromised Metabolics in and Degeneration of Locus Ceruleus Neurons. *J Neurosci*. 2014;34(12):4418-4431. doi:10.1523/JNEUROSCI.5025-12.2014.

6. de Vivo L, Nelson AB, Bellesi M, Noguti J, Tononi G, Cirelli C. Loss of Sleep Affects the Ultrastructure of Pyramidal Neurons in the Adolescent Mouse Frontal Cortex. *Sleep*. 2016;39(4):861-874. doi:10.5665/sleep.5644.

7. Naidoo N, Giang W, Galante RJ, Pack AI. Sleep deprivation induces the unfolded protein response in mouse cerebral cortex. *J Neurochem*. 2005;92(5):1150-1157. doi:10.1111/j.1471-4159.2004.02952.x.

8. Xie L, Kang H, Xu Q, et al. Sleep drives metabolite clearance from the adult brain. *Science*. 2013;342(6156):373-377. doi:10.1126/science.1241224.

9. Dash MB, Douglas CL, Vyazovskiy VV, Cirelli C, Tononi G. Long-Term Homeostasis of Extracellular Glutamate in the Rat Cerebral Cortex across Sleep and Waking States. *J Neurosci*. 2009;29(3):620-629. doi:10.1523/JNEUROSCI.5486-08.2009.

10. Naylor E, Aillon DV, Gabbert S, et al. Simultaneous real-time measurement of EEG/EMG and L-glutamate in mice: A biosensor study of neuronal activity during sleep. *J Electroanal Chem Lausanne Switz*. 2011;656(1-2):106-113. doi:10.1016/j.jelechem.2010.12.031.

11. Bellesi M, Pfister-Genskow M, Maret S, Keles S, Tononi G, Cirelli C. Effects of Sleep and Wake on Oligodendrocytes and Their Precursors. *J Neurosci*. 2013;33(36):14288-14300. doi:10.1523/JNEUROSCI.5102-12.2013.

12. Yoshikawa F, Sato Y, Tohyama K, et al. Opalin, a Transmembrane Sialylglycoprotein Located in the Central Nervous System Myelin Paranodal Loop Membrane. *J Biol Chem*. 2008;283(30):20830-20840. doi:10.1074/jbc.M801314200.

13. Yaffe Y, Hugger I, Yassaf IN, et al. The myelin proteolipid plasmolipin forms oligomers and induces liquid-ordered membranes in the Golgi complex. *J Cell Sci*. 2015;128(13):2293-2302. doi:10.1242/jcs.166249.

14. Zearfoss NR, Farley BM, Ryder SP. Post-transcriptional regulation of myelin formation. *Biochim Biophys Acta BBA - Gene Regul Mech*. 2008;1779(8):486-494. doi:10.1016/j.bbagrm.2008.06.003.

15. Elvsåshagen T, Norbom LB, Pedersen PØ, et al. Widespread changes in white matter microstructure after a day of waking and sleep deprivation. *PloS One*. 2015;10(5):e0127351. doi:10.1371/journal.pone.0127351.

16. Li S, Tian J, Bauer A, et al. Reduced Integrity of Right Lateralized White Matter in Patients with Primary Insomnia: A Diffusion-Tensor Imaging Study. *Radiology*. April 2016:152038. doi:10.1148/radiol.2016152038.

17. Sexton CE, Zsoldos E, Filippini N, et al. Associations between self-reported sleep quality and white matter in community-dwelling older adults: A prospective cohort study. *Hum Brain Mapp*.:n/a-n/a. doi:10.1002/hbm.23739.

18. Fields RD. White matter in learning, cognition and psychiatric disorders. *Trends Neurosci*. 2008;31(7):361-370. doi:10.1016/j.tins.2008.04.001.

19. Feng G, Mellor RH, Bernstein M, et al. Imaging Neuronal Subsets in Transgenic Mice Expressing Multiple Spectral Variants of GFP. *Neuron*. 2000;28(1):41-51. doi:10.1016/S0896-6273(00)00084-2.

20. Maret S, Faraguna U, Nelson AB, Cirelli C, Tononi G. Sleep and waking modulate spine turnover in the adolescent mouse cortex. *Nat Neurosci*. 2011;14(11):1418-1420. doi:10.1038/nn.2934.

21. Nelson AB, Faraguna U, Zoltan JT, Tononi G, Cirelli C. Sleep Patterns and Homeostatic Mechanisms in Adolescent Mice. *Brain Sci*. 2013;3(1):318-343. doi:10.3390/brainsci3010318.

22. de Vivo L, Faraguna U, Nelson AB, et al. Developmental Patterns of Sleep Slow Wave Activity and Synaptic Density in Adolescent Mice. *Sleep*. 2014;37(4):689-700. doi:10.5665/sleep.3570.

23. de Vivo L, Bellesi M, Marshall W, et al. Ultrastructural evidence for synaptic scaling across the wake/sleep cycle. *Science*. 2017;355(6324):507-510. doi:10.1126/science.aah5982.

24. Inaki K, Nishimura S, Nakashiba T, Itohara S, Yoshihara Y. Laminar organization of the developing lateral olfactory tract revealed by differential expression of cell recognition molecules. *J Comp Neurol*. 2004;479(3):243-256. doi:10.1002/cne.20270.

25. Laird NM, Ware JH. Random-effects models for longitudinal data. *Biometrics*. 1982;38(4):963-974.

26. Mitzel HC, Games PA. Circularity and multiple comparisons in repeated measure designs. *Br J Math Stat Psychol*. 1981;34(2):253-259. doi:10.1111/j.2044-8317.1981.tb00635.x.

27. Barr DJ. Random effects structure for testing interactions in linear mixed-effects models. *Front Psychol*. 2013;4. doi:10.3389/fpsyg.2013.00328.

28. Bates D, Maechler M, Bolker B, Walker S. Fitting Linear Mixed-Effects Models Using lme4. *J Stat Softw*. 2015;67(1):1–48. doi:10.18637/jss.v067.i01.

29. Bretz F, Hothorn T, Westfall PH, others. *Multiple Comparisons Using R*. CRC Press Boca Raton; 2011.

30. Ibrahim M, Butt AM, Berry M. Relationship between myelin sheath diameter and internodal length in axons of the anterior medullary velum of the adult rat. *J Neurol Sci*. 1995;133(1–2):119-127. doi:10.1016/0022-510X(95)00174-Z.

31. Chomiak T, Hu B. What Is the Optimal Value of the g-Ratio for Myelinated Fibers in the Rat CNS? A Theoretical Approach. *PLOS ONE*. 2009;4(11):e7754. doi:10.1371/journal.pone.0007754.

32. Waxman SG, Bennett MV. Relative conduction velocities of small myelinated and non-myelinated fibres in the central nervous system. *Nature New Biol*. 1972;238(85):217-219.

33. Pajevic S, Basser PJ, Fields RD. Role of myelin plasticity in oscillations and synchrony of neuronal activity. *Neuroscience*. 2014;276:135-147. doi:10.1016/j.neuroscience.2013.11.007.

34. Cirelli C, Faraguna U, Tononi G. Changes in brain gene expression after long-term sleep deprivation. *J Neurochem*. 2006;98(5):1632-1645. doi:10.1111/j.1471-4159.2006.04058.x.

35. Mongrain V, Hernandez SA, Pradervand S, et al. Separating the Contribution of Glucocorticoids and Wakefulness to the Molecular and Electrophysiological Correlates of Sleep Homeostasis. *Sleep*. 2010;33(9):1147-1157.

36. Harris JJ, Attwell D. The Energetics of CNS White Matter. *J Neurosci*. 2012;32(1):356-371. doi:10.1523/JNEUROSCI.3430-11.2012.

37. Fünfschilling U, Supplie LM, Mahad D, et al. Glycolytic oligodendrocytes maintain myelin and long-term axonal integrity. *Nature*. 2012;485(7399):517-521. doi:10.1038/nature11007.

38. Lee Y, Morrison BM, Li Y, et al. Oligodendroglia metabolically support axons and contribute to neurodegeneration. *Nature*. 2012;487(7408):443-448. doi:10.1038/nature11314.

39. Saab AS, Tzvetanova ID, Nave K-A. The role of myelin and oligodendrocytes in axonal energy metabolism. *Curr Opin Neurobiol*. 2013;23(6):1065-1072. doi:10.1016/j.conb.2013.09.008.

40. Rinholm JE, Hamilton NB, Kessaris N, Richardson WD, Bergersen LH, Attwell D. Regulation of Oligodendrocyte Development and Myelination by Glucose and Lactate. *J Neurosci*. 2011;31(2):538-548. doi:10.1523/JNEUROSCI.3516-10.2011.

41. Dash MB, Tononi G, Cirelli C. Extracellular Levels of Lactate, but Not Oxygen, Reflect Sleep Homeostasis in the Rat Cerebral Cortex. *Sleep*. 2012;35(7):909-919. doi:10.5665/sleep.1950.

42. Gibson EM, Purger D, Mount CW, et al. Neuronal Activity Promotes Oligodendrogenesis and Adaptive Myelination in the Mammalian Brain. *Science*. 2014;344(6183):1252304. doi:10.1126/science.1252304.

43. McKenzie IA, Ohayon D, Li H, et al. Motor skill learning requires active central myelination. *Science*. 2014;346(6207):318-322. doi:10.1126/science.1254960.

44. Liu J, Dietz K, DeLoyht JM, et al. Impaired adult myelination in the prefrontal cortex of socially isolated mice. *Nat Neurosci*. 2012;15(12):1621-1623. doi:10.1038/nn.3263.

45. Blumenfeld-Katzir T, Pasternak O, Dagan M, Assaf Y. Diffusion MRI of Structural Brain Plasticity Induced by a Learning and Memory Task. *PLOS ONE*. 2011;6(6):e20678. doi:10.1371/journal.pone.0020678.

46. Sampaio-Baptista C, Khrapitchev AA, Foxley S, et al. Motor Skill Learning Induces Changes in White Matter Microstructure and Myelination. *J Neurosci*. 2013;33(50):19499-19503. doi:10.1523/JNEUROSCI.3048-13.2013.

47. Hofstetter S, Tavor I, Moryosef ST, Assaf Y. Short-Term Learning Induces White Matter Plasticity in the Fornix. *J Neurosci*. 2013;33(31):12844-12850. doi:10.1523/JNEUROSCI.4520-12.2013.

48. Miyata S, Koyama Y, Takemoto K, et al. Plasma Corticosterone Activates SGK1 and Induces Morphological Changes in Oligodendrocytes in Corpus Callosum. *PLOS ONE*. 2011;6(5):e19859. doi:10.1371/journal.pone.0019859.

49. Yamamoto A, Yasuno F, Iida H, et al. Association between chronic stress-induced structural abnormalities in Ranvier nodes and reduced oligodendrocyte activity in major depression. *Sci Rep*. 2016;6:23084. doi:10.1038/srep23084.

50. Liu J, Dietz K, Hodes GE, Russo SJ, Casaccia P. Widespread transcriptional alternations in oligodendrocytes in the adult mouse brain following chronic stress. *Dev Neurobiol*. September 2017. doi:10.1002/dneu.22533.

51. Bohn MC, Friedrich VL. Recovery of myelination in rat optic nerve after developmental retardation by cortisol. *J Neurosci*. 1982;2(9):1292-1298.

52. Dunlop SA, Archer MA, Quinlivan JA, Beazley LD, Newnham JP. Repeated Prenatal Corticosteroids Delay Myelination in the Ovine Central Nervous System. *J Matern Fetal Med*. 1997;6(6):309-313. doi:10.3109/14767059709162011.

53. Meyer JS, Fairman KR. Early adrenalectomy increases myelin content of the rat brain. *Dev Brain Res*. 1985;17(1–2):1-9. doi:10.1016/0165-3806(85)90126-9.

54. Meyer JS, Fairman KR. Adrenalectomy in the developing rat: Does it cause reduced or increased brain myelination? *Dev Psychobiol*. 1985;18(4):349-354. doi:10.1002/dev.420180407.

55. Everson CA, Gilliland MA, Kushida CA, et al. Sleep deprivation in the rat: IX. Recovery. *Sleep*. 1989;12(1):60-67.

56. Pejovic S, Basta M, Vgontzas AN, et al. Effects of recovery sleep after one work week of mild sleep restriction on interleukin-6 and cortisol secretion and daytime sleepiness and performance. *Am J Physiol - Endocrinol Metab*. 2013;305(7):E890-E896. doi:10.1152/ajpendo.00301.2013.

57. Meerlo P, Koehl M, van der Borght K, Turek FW. Sleep restriction alters the hypothalamic-pituitary-adrenal response to stress. *J Neuroendocrinol*. 2002;14(5):397-402.

58. Palchykova S, Winsky-Sommerer R, Meerlo P, Dürr R, Tobler I. Sleep deprivation impairs object recognition in mice. *Neurobiol Learn Mem*. 2006;85(3):263-271. doi:10.1016/j.nlm.2005.11.005.

59. Grissom N, Bhatnagar S. Habituation to repeated stress: get used to it. *Neurobiol Learn Mem*. 2009;92(2):215-224. doi:10.1016/j.nlm.2008.07.001.

60. Babb JA, Masini CV, Day HEW, Campeau S. Habituation of hypothalamic-pituitary-adrenocortical axis hormones to repeated homotypic stress and subsequent heterotypic stressor exposure in male and female rats. *Stress Amst Neth*. 2014;17(3):224-234. doi:10.3109/10253890.2014.905534.

61. Polak PE, Kalinin S, Feinstein DL. Locus coeruleus damage and noradrenaline reductions in multiple sclerosis and experimental autoimmune encephalomyelitis. *Brain J Neurol*. 2011;134(Pt 3):665-677. doi:10.1093/brain/awq362.

62. Simonini MV, Polak PE, Sharp A, McGuire S, Galea E, Feinstein DL. Increasing CNS noradrenaline reduces EAE severity. *J Neuroimmune Pharmacol Off J Soc NeuroImmune Pharmacol*. 2010;5(2):252-259. doi:10.1007/s11481-009-9182-2.

63. Hildebrand C, Hahn R. Relation between myelin sheath thickness and axon size in spinal cord white matter of some vertebrate species. *J Neurol Sci*. 1978;38(3):421-434.

64. Murray JA, Blakemore WF. The relationship between internodal length and fibre diameter in the spinal cord of the cat. *J Neurol Sci*. 1980;45(1):29-41.

65. de Paula Faria D, de Vries EFJ, Sijbesma JWA, Dierckx RAJO, Buchpiguel CA, Copray S. PET imaging of demyelination and remyelination in the cuprizone mouse model for multiple sclerosis: a comparison between [11C]CIC and [11C]MeDAS. *NeuroImage*. 2014;87:395-402. doi:10.1016/j.neuroimage.2013.10.057.

66. Veronese M, Bodini B, García-Lorenzo D, et al. Quantification of [(11)C]PIB PET for imaging myelin in the human brain: a test-retest reproducibility study in high-resolution research tomography. *J Cereb Blood Flow Metab Off J Int Soc Cereb Blood Flow Metab*. 2015;35(11):1771-1782. doi:10.1038/jcbfm.2015.120.